Journal of Power Sources 194 (2009) 697–703

Contents lists available at ScienceDirect

Journal of Power Sources

journal homepage: www.elsevier.com/locate/jpowsour

Numerical study to examine the performance of multi-pass serpentine flow-fields for cooling plates in polymer electrolyte membrane fuel cells

Seung Ho Yu [a], Sangho Sohn [a,*], Jin Hyun Nam [b], Charn-Jung Kim [a]

[a] School of Mechanical and Aerospace Engineering, Seoul National University, Seoul 151-744, Republic of Korea
[b] School of Mechanical and Automotive Engineering, Kookmin University, Seoul 136-702, Republic of Korea

ARTICLE INFO

Article history:
Received 20 March 2009
Received in revised form 24 April 2009
Accepted 1 June 2009
Available online 18 June 2009

Keywords:
Polymer electrolyte membrane fuel cell
Cooling plate
Coolant flow channel
Multi-pass serpentine flow-fields
Temperature uniformity
Heat management

ABSTRACT

Temperature is an important factor that impacts the performance of polymer electrolyte membrane fuel cells (PEMFCs). Proper cooling systems are indispensable for heat management. Cooling plates with coolant flow channels are mainly used to release the reaction heat in PEMFCs and thus control their operating temperature. In this study, several multi-pass serpentine flow-field (MPSFF) designs are studied in order to achieve better heat management by using cooling plates. Based on computational fluid dynamics (CFD) simulations of fluid flow and heat transfer in the cooling plates, the cooling performance of the six serpentine channel designs is evaluated. The results demonstrate that MPSFFs lead to better cooling performance compared with a conventional serpentine flow-field, in terms of both the maximum temperature and temperature uniformity. The effect of the Reynolds number and heat flux on the cooling performance exhibited by the six designs is also investigated.

1. Introduction

Fuel cells are energy conversion devices that directly convert the chemical energy of fuels into electrical energy via electrochemical reactions. Fuel cells are expected to because important power sources due to their higher efficiency and cleaner emissions as compared with conventional heat engines. Polymer electrolyte membrane fuel cells (PEMFCs) exhibit a high power density and a short start-up time. The technology also operates at a low temperature of less than 100 °C. Studies have been conducted on for many applications that include various systems in the automotive industry, portable electronic devices, and stationary power generation [1–4].

Since heat is continuously generated as the by-product of the electrochemical reactions, proper heat management is essential to ensure good performance from PEMFCs. Overheating and non-uniform heating are two of the main problems. Prolonged operation of PEMFCs at high temperatures causes increased ohmic resistance due to membrane dehydration that in turn, leads to performance loss and degradation. In addition, non-uniform temperature distributions result in spatial variations of the reaction rate that lead to a reduction in the durability of PEMFC hardware. Therefore, proper cooling is necessary to control the operating temperature and to maintain a uniform temperature distribution [5,6].

Cooling plates with coolant flow channels that are designed for better PEMFC heat management have recently been investigated [7,8]. The cooling performance of several serpentine and parallel channel designs was evaluated in [7,8] through a numerical simulation of fluid flow and heat transfer within the cooling plates. Cooling plates with serpentine flow-fields generally exhibited better performance in terms of temperature uniformity and maximum temperature, as compared with those with parallel flow-fields.

Recently, a convection-enhanced serpentine flow-field (CESFF) was proposed by Xu and Zhao [9]. This design was shown to enhance under-rib convection (convective flow under bipolar plate ribs) and thereby improve the performance of a direct methanol fuel cell (DMFC). More recently, Nam et al. [10] noticed the geometrical similarity between the flow-field designs for coolant channels in [7,8] and in the CESFF [9]. This led to the proposal of a simple design to generate multi-pass serpentine flow-fields (MPSFFs). Based on geometrical characterizations, Nam et al. [10] showed that MPSFFs can enhance under-rib convection when used as reactant channels and can improve temperature uniformity when used as coolant channels.

In the present study, six types of serpentine channel design (a conventional serpentine flow field, four MPSFFs, and a spiral flow field) are evaluated as coolant flow-fields for cooling plates. Computational fluid dynamics (CFD) is used to model accurately the effects of fluid flow and heat transfer. Assessment of the performance of the cooling plates is based on the maximum surface temperature and the temperature uniformity index as obtained by CFD calculations.

* Corresponding author. Tel.: +82 2 880 1656; fax: +82 2 883 0179.
E-mail address: son35@snu.ac.kr (S. Sohn).

0378-7753/$ – see front matter © 2009 Elsevier B.V. All rights reserved.
doi:10.1016/j.jpowsour.2009.06.025

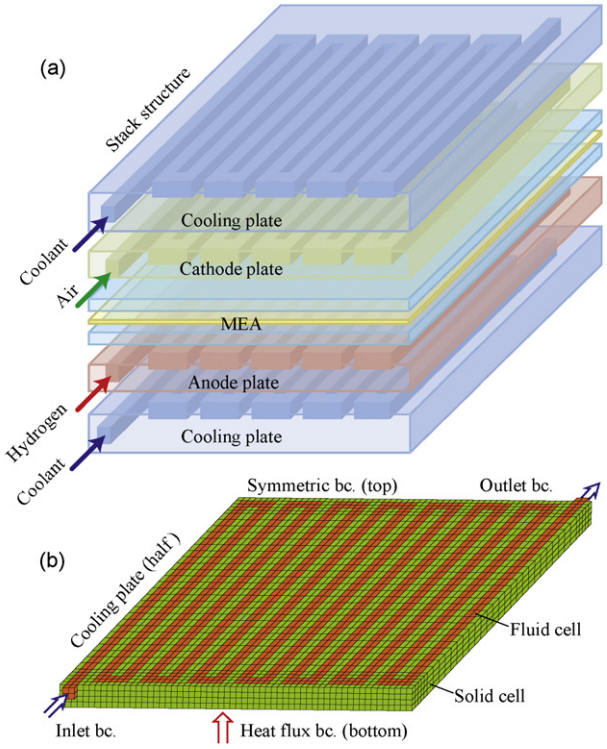

Fig. 1. Stack structure of PEMFC with cooling plates: (a) stack structure and (b) cooling plate (half domain).

2. Theory and calculations

To ensure proper levels of output power, PEMFCs are generally constructed by stacking up multiple individual cells [2]. The modular single cell consists of a membrane electrode assembly (MEA) and two bipolar plates. The stacked PEMFC structure, including the two cooling plates that are used to expel the reaction heat, is shown in Fig. 1(a). The role of the bipolar plates is to conduct electrons through their solid structure and to supply reactants and remove exhaust products through the gas channels formed on the surface. The MEA is the location of the actual electrochemical reactions, which produce electricity and heat.

A cooling plate installed between every two cells is shown in Fig. 1(a). This arrangement corresponds to a number of cooling channels per cell, n, of about 1. In practice, however, an n of about 3–5 is generally used [8]. The heat flux, q, that should be exhausted by a cooling plate at steady-state is calculated as [8]

$$q = \frac{Q}{A} = \frac{nI(-\Delta h_f^o/2F - V)}{A}, \quad (1)$$

where I is the cell current; V is the output cell voltage; A is the cell area; Δh_f^o is the formation enthalpy of water (−241.8 and −285.8 kJ mol^{-1} for the power and higher heating values, respectively), and F is the Faraday constant (96,487 C mol^{-1}). Given that the thermal efficiency is around 40–50%, the heat production inside PEMFCs is comparable with the output cell power (about 1–1.5 kW of heat is produced in PEMFCs that have a rated power of 1 kW).

Due to the symmetric structure of the cooling plate, only a half domain was required for the CFD cooling plate simulations. The calculation domain considered in this study is shown in Fig. 1(b), where a symmetric boundary and a constant heat flux boundary are also illustrated. Note that only half of the total heat flux q in Eq. (1) should be imposed on the constant heat flux boundary. In this study, a value of q of 2000–8000 W m^{-2} is considered; this is believed to be within the range encountered during normal PEMFC operation.

Table 1
Parameters used for cooling plate simulations.

Parameters	Values
Plate geometries	
Dimension, $l_p \times w_p \times t_p$	60 mm × 60 mm × 2 mm
Channel and rib width, w_{ch} or w_{rib}	2 mm
Channel depth, t_{ch}	1 mm
Hydraulic diameter, D_h	1.33 mm
Properties of plate (graphite)	
Density, ρ_p	2250 kg m^{-3}
Specific heat, $c_{p,p}$	690 J kg^{-1} K^{-1}
Thermal conductivity, k_p	24.0 W m^{-1} K^{-1}
Properties of coolant (water) at 40 °C	
Density, ρ_w	992.2 kg m^{-3}
Specific heat, $c_{p,w}$	4179 J kg^{-1} K^{-1}
Thermal conductivity, k_w	0.62 W m^{-1} K^{-1}
Viscosity, μ_w	0.000653 Pa s
Operating conditions[a]	
Heat flux, q	2000, 5000, 8000 W m^{-2}
Inlet fluid temperature, T_{in}	40 °C
Inlet fluid velocity, u_{in}	0.25, 0.375, 0.5, 0.625, 0.75, 0.875, 1 m s^{-1}
Reynolds number, $Re = \rho_w \mu_{in} D_h / \mu_w$	506, 760, 1013, 1266, 1519, 1773, 2026

[a] Underlined text denotes standard conditions.

Six of the serpentine flow-fields that are considered coolant channels in this study are shown in Fig. 2. Models A and F correspond to a conventional serpentine flow-field and a conventional spiral flow-field, respectively. Models B, C, D and E are the previously proposed MPSFFs that were used to facilitate under-rib convection in PEMFCs as reported elsewhere [10]. Other researchers have suggested that these MPSFFs may be used to enhance the spatial uniformity of the temperature distribution in the cooling plates by facilitating the heat transfer between channels that are positioned at significantly different flow distances from the inlet. Table 1 summarizes the geometrical parameters for the cooling plates along with the physical properties of the plate material (graphite) and the coolant fluid (water) [11].

Calculations of the fluid flow and heat transfer in the cooling plates were conducted using a commercial CFD program, Star-CD (CD-Adapco Group, USA). This program primarily solves the governing equations for the conservation of mass, momentum, and energy in fluids. For the laminar flow ($Re < 2300$) of a Newtonian incompressible fluid (water), the governing equations can be summarized as

$$\frac{\partial u_j}{\partial x_j} = 0, \quad (2)$$

$$\rho\left(\frac{\partial u_i}{\partial t} + u_j\frac{\partial u_i}{\partial x_j}\right) = -\frac{\partial p}{\partial x_i} + \frac{\partial}{\partial x_j}\left(\mu\frac{\partial u_i}{\partial x_j}\right), \quad (3)$$

$$\rho c_p\left(\frac{\partial T}{\partial t} + u_j\frac{\partial T}{\partial x_j}\right) = \frac{\partial}{\partial x_j}\left(k\frac{\partial T}{\partial x_j}\right), \quad (4)$$

where ρ is the density; μ is the viscosity; c_p is the specific heat; k is the density of the cooling fluid. Since this study focuses on steady cooling performance, the transient terms $\partial(\cdot)/\partial t$ in Eqs. (3) and (4) are not considered. For solid regions within the cooling plates, only the energy equation, Eq. (4), is considered for the case of zero fluid velocity ($u = 0$).

The SIMPLE algorithm was used to solve the coupling of the continuity equation, Eq. (2), and the Navier–Stokes equation, Eq. (3). The solution was assumed to converge when the residuals of all of the governing equations were reduced below 0.0001 during a series of iterative calculations. The operating conditions used in the CFD

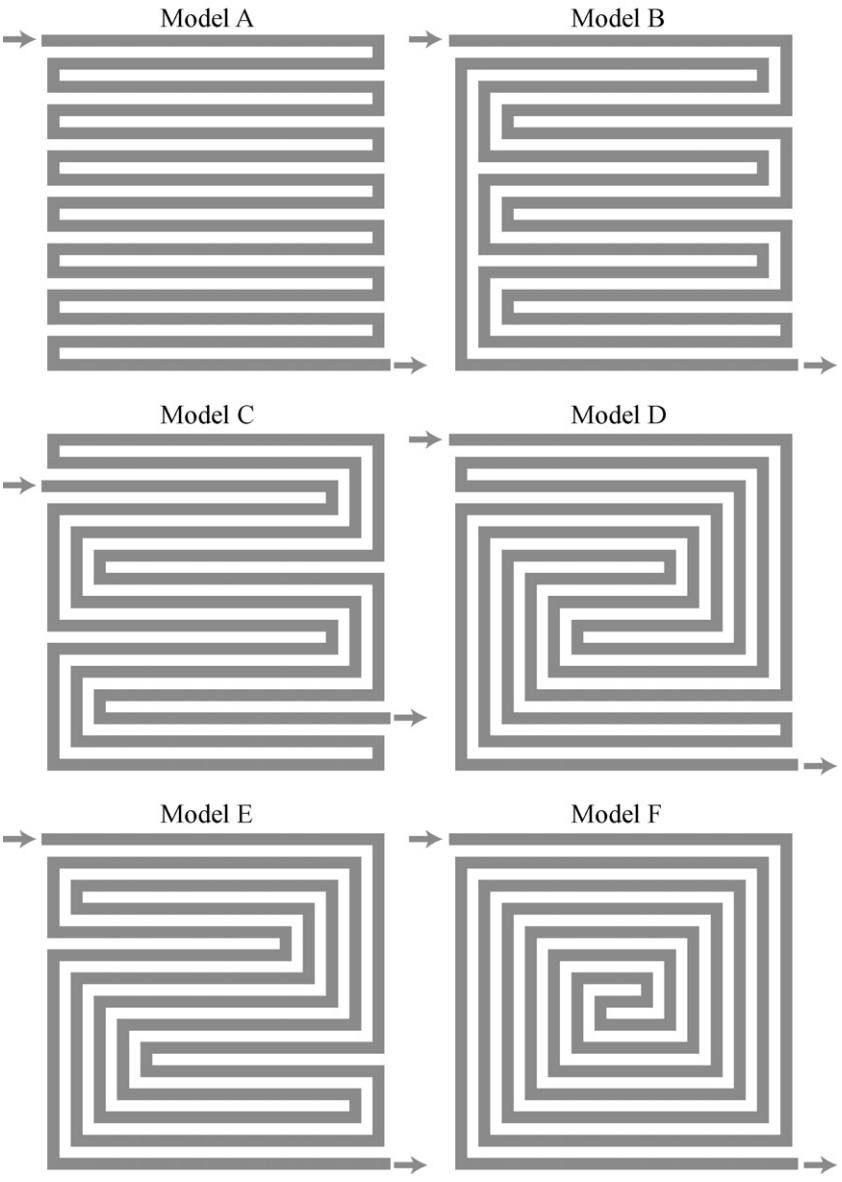

Fig. 2. Six serpentine flow-fields used as coolant channels.

simulations are listed in Table 1, where underlined text denotes standard conditions.

3. Results and discussion

Although CFD is an accurate method to solve thermo-fluid problems, it is also computationally expensive. Thus, a series of grid dependence tests for all six flow fields were first conducted to determine the optimum grid densities for a solution that would be both accurate and efficient. The predicted maximum temperature in, and the pressure drop through, a cooling plate with a conventional serpentine flow-field (Model A) are shown in Fig. 3 as functions of the number of finite volume cells used in the CFD simulation. To obtain Fig. 3, the inlet temperature, T_{in}, and the velocity, u_{in}, of water were fixed at 40 °C and 1 m s^{-1} (Re = 1013), respectively. It is noted that a higher Reynolds number generally requires a higher grid density.

The predicted results become less dependent on the cell number when that number exceeds 400,000, as shown in Fig. 3. The results suggest that a cell number of 400,000 is sufficient to obtain grid-independent solutions. Grid-dependence tests for the other

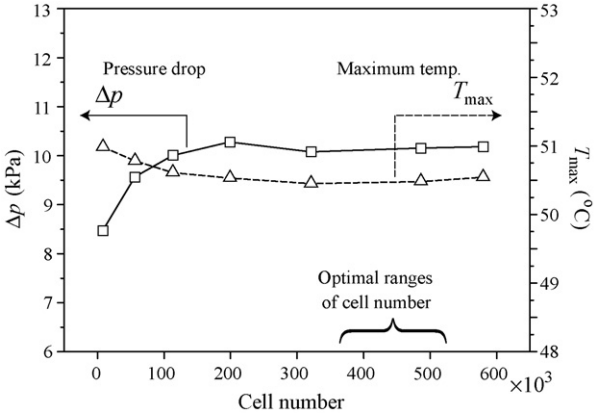

Fig. 3. Results of grid dependence test for conventional serpentine-flow (Model A) at Re = 1013.

Table 2
Results of CFD simulations conducted for six serpentine flow-fields under standard operating conditions (Re = 1013).

Channel design	Cell number[a]	T_{max} (°C)	T_{min} (°C)	T_{avg} (°C)	ΔT (°C)	U_T (°C)	Δp (Pa)
Model A	486000	50.5	40.9	45.9	9.57	2.14	10,154
Model B	379290	49.0	41.3	46.7	7.71	1.19	11,537
Model C	422330	48.5	41.5	46.2	7.01	1.26	11,780
Model D	532800	47.1	41.2	45.3	5.92	0.92	12,393
Model E	468000	47.1	41.2	45.6	5.89	0.88	12,291
Model F	432630	48.0	41.3	46.7	6.71	0.97	12,331

[a] Optimized numbers of finite volume cells were chosen after grid dependence tests were conducted for Re = 1013.

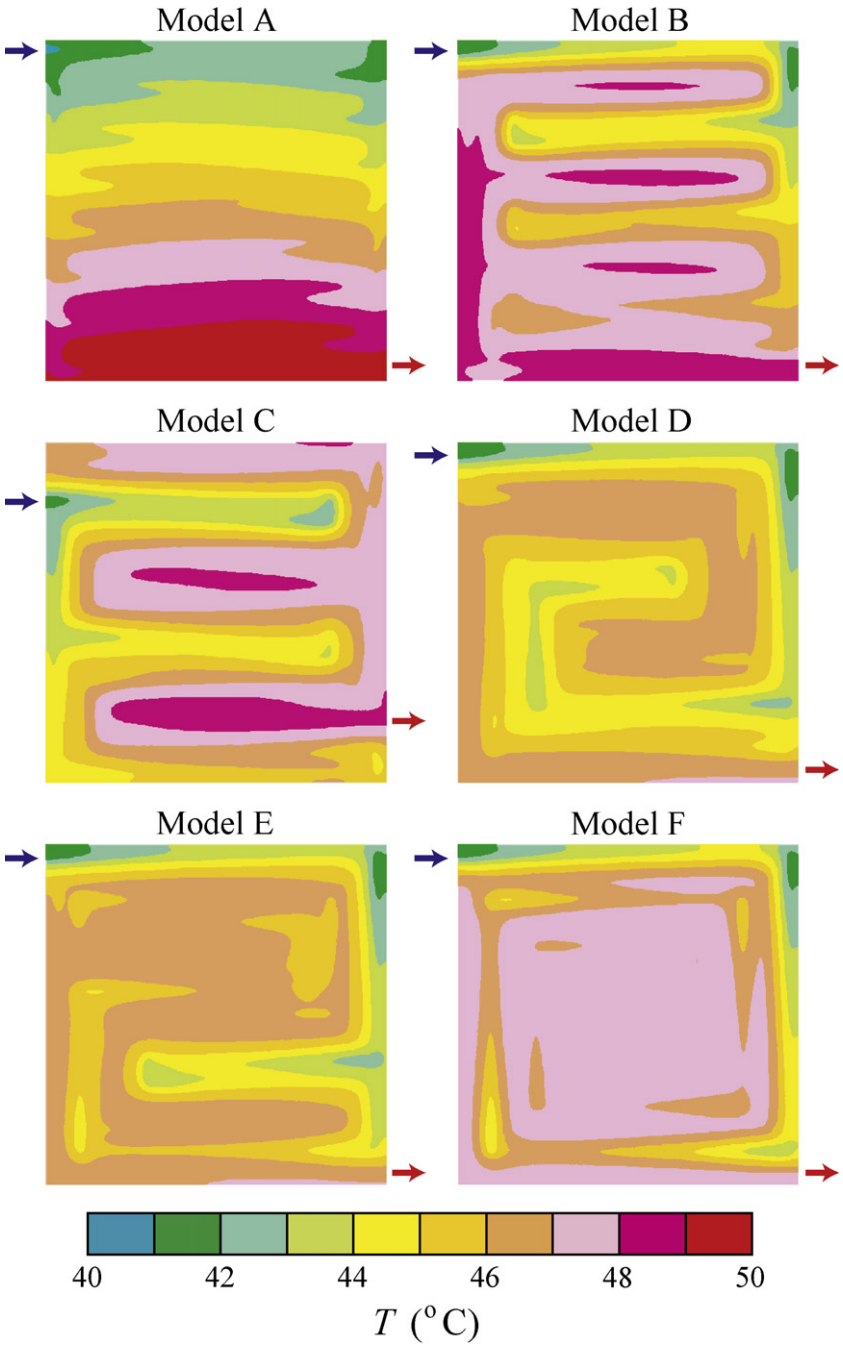

Fig. 4. Temperature distribution in cooling plates under standard operating conditions (Re = 1013).

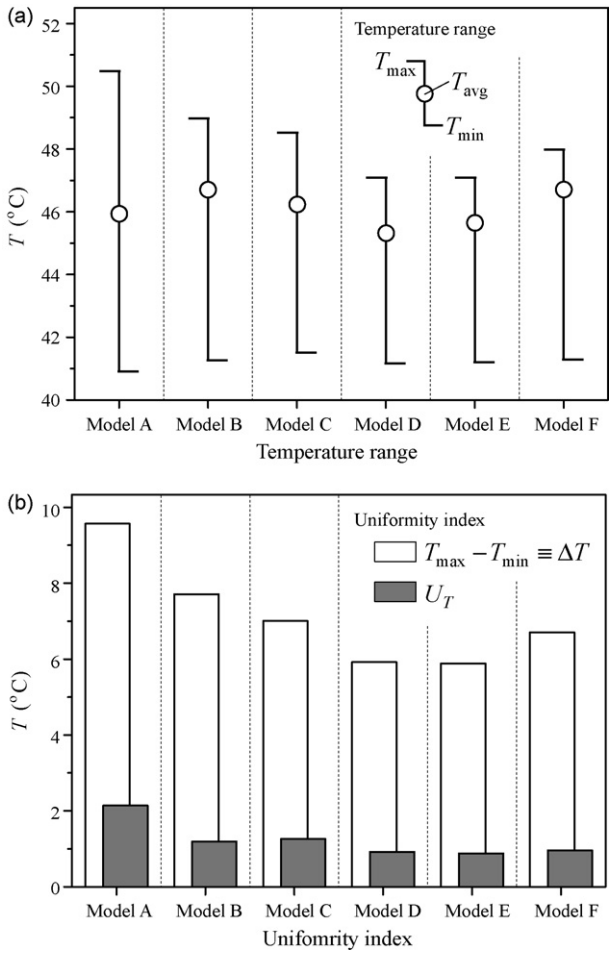

Fig. 5. Temperature uniformity indices for cooling plates under standard operating conditions (Re = 1013): (a) surface temperature ranges and (b) temperature uniformity indices.

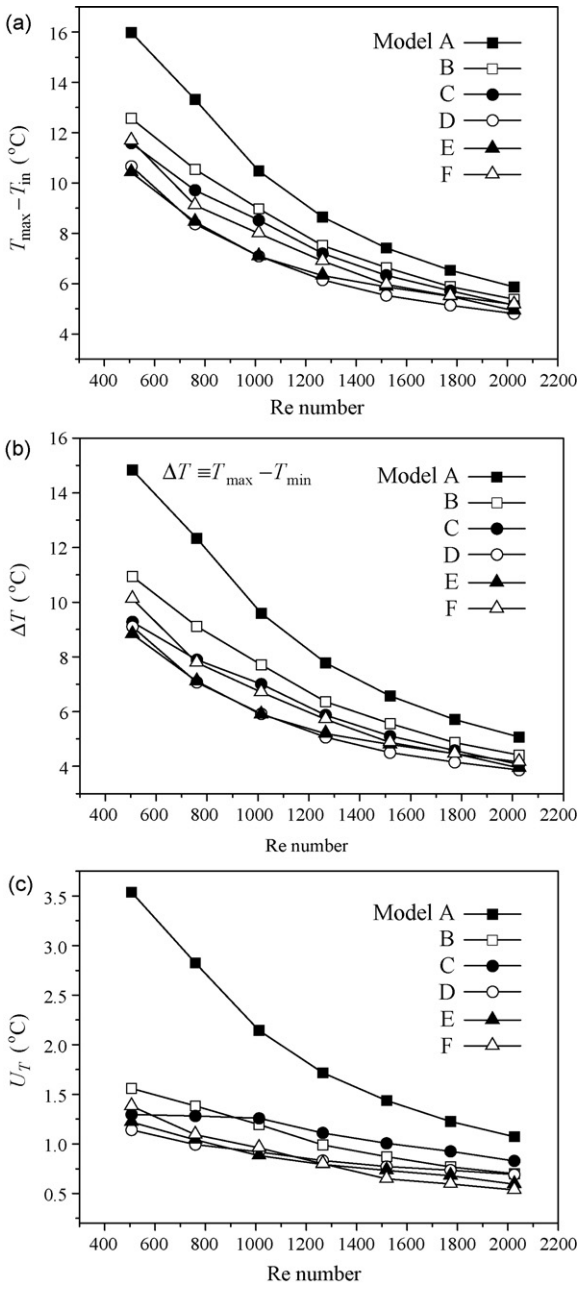

Fig. 6. Effects of flow velocity, u_{in}, on performance of cooling plates: (a) maximum surface temperature, T_{max}; (b) surface temperature difference, ΔT; and (c) temperature uniformity index, U_T.

flow-fields also show that about 400,000 volume cells are sufficient to obtain converged results. The optimized cell numbers used in our CFD simulations are summarized in Table 2. Note that the grid density is higher near the corner regions of the flow-fields than in the straight regions.

3.1. Effect of channel design

The role of the cooling plate is to release heat from electrochemical reactions and to maintain a uniform temperature distribution within the MEA. A uniform temperature distribution is particularly desirable at the surface (interface) between the cooling plate and the anode or cathode plate. The simulated surface temperature distributions for six flow-field designs under standard operating conditions (Re = 1013) are presented in Fig. 4. The distribution illustrates a trend according to which the surface temperature increases along the flow channel from the inlet region to the outlet region. This is due to a somewhat constant increase in coolant temperature along the channel. The data also show that the conventional serpentine flow-field gives a more non-uniform temperature distribution than do the other flow-fields considered in this study.

Several indices related to the uniformity of the temperature distribution were calculated to arrive at a better quantified evaluation of the effects of each flow-field design. The temperature uniformity index, U_T, is defined as

$$U_T = \frac{\int_V |T - T_{avg}| dV}{\int_V dV}, \quad (5)$$

where V is the volume and T_{avg} is the average surface temperature, defined as

$$T_{avg} = \frac{\int_V T dV}{\int_V dV}. \quad (6)$$

The summations in Eqs. (5) and (6) are conducted for only those surface volume cells that are in contact with the constant heat flux boundary. The surface temperature difference, $\Delta T (\equiv T_{max} - T_{min})$, is another important index to measure temperature uniformity, where T_{max} and T_{min} are the maximum and minimum surface tem-

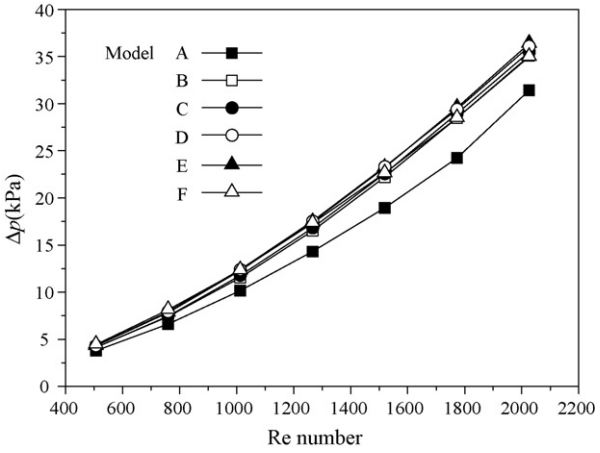

Fig. 7. Effect of flow velocity, u_{in}, on pressure drop, Δp, through cooling plates.

peratures, respectively. It is noted that coolant flow-fields should be designed to have smaller U_T and ΔT values.

Quantified summaries of the effects of channel design along with the pressure drop, Δp, in each flow field ($Re = 1013$) are provided in Table 2. These data are also presented graphically in Fig. 5 for direct comparison. The results clearly indicate poor cooling performance for the conventional serpentine flow-field design (Model A) when applied to coolant flow channels. The uniformity indices for the four MPSFFs (Models B–E) and the conventional spiral flow-field (Model F) are much smaller than those for the conventional serpentine flow-field. The reduction is estimated to reach 38% for ΔT and 59% for U_T. The most uniform temperature distribution is obtained for Model E. In addition, the enhancement of temperature uniformity within MPSFFs and for the spiral flow-field is due to the decrease in T_{max} and the increase in T_{min}. In Table 2, the pressure drop, Δp, is lower in the cooling plate with the conventional serpentine flow-field than in the plates with the other flow-fields. The greater pressure drop with MPSFFs and the spiral flow-field is due to the more complex flow patterns in these fields.

3.2. Effect of flow velocity

The effect of flow velocity, u_{in}, on the cooling performance of the flow-fields was examined by varying u_{in} from 0.25 to 1 m s^{-1}. These velocities correspond to a Reynolds number range of 506–2026, as listed in Table 2. The data in Fig. 6 show that the uniformity index decreases as Re increases. A higher coolant velocity is favorable for the release of reaction heat due to an increase in thermal mass, as well as an enhancement of the convective heat transfer. In Fig. 6, the conventional serpentine flow-field (Model A) exhibits a weaker cooling performance than the MPSFFs (Models B–E) and the spiral flow-field (Model F); this discrepancy becomes smaller as Re increases.

The pressure drop, Δp, is an important factor that should always be considered in designing cooling plates. As shown in Fig. 6, a higher u_{in} in the cooling plates leads to better cooling performance in terms of temperature uniformity; but, this also requires higher power consumption to pump the cooling fluid through the cooling plates more quickly. The predicted pressure drop, Δp, through six serpentine flow-fields is shown in Fig. 7, where Δp increases as the Reynolds number increases. The non-linear correlation between Δp and Re is believed to be caused by the secondary pressure losses in the 90° and 180° bends in these flow-fields. The conventional serpentine flow-field (Model A) exhibits the lowest pressure drop, while the other flow-fields showed slightly greater pressure drops (elevations of about 10%).

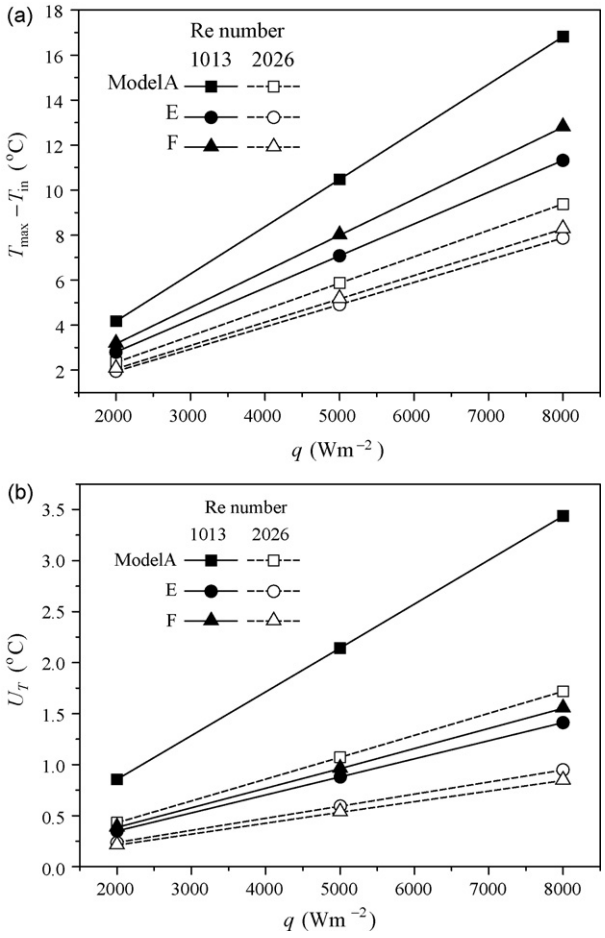

Fig. 8. Effect of heat flux, q, on performance of cooling plates: (a) maximum surface temperature, T_{max} and (b) temperature uniformity index, U_T.

3.3. Effect of heat flux

The performance of the cooling plates was examined by varying the heat flux, q, between 2000, 5000 and 8000 W m^{-2}. The conventional serpentine flow-field (Model A), a MPSFF (Model E) and the spiral flow-field (Model F) were investigated. The variation in the maximum temperature, T_{max}, and the temperature uniformity index, U_T, as a function of the heat flux is presented in Fig. 8. The values of T_{max} and U_T seem to be perfectly proportional to the prescribed q. In fact, U_T/q is found to be almost constant for each flow-field, irrespective of the prescribed heat flux value. A higher Reynolds number generally results in a lower U_T/q due to an enhanced convective heat transfer rate between the solid surface and the coolant fluid.

4. Conclusion

The performance of cooling plates with different coolant channel designs was evaluated by simulating the fluid flow and heat transfer using CFD. The following indices were calculated and compared, all of which are dependent on temperature distribution uniformity: the maximum temperature, T_{max}, the temperature difference, ΔT, and the temperature uniformity index, U_T. The simulation results suggest that the conventional serpentine flow-field (Model A) gives the largest T_{max}, ΔT, and U_T of the six flow fields considered in this study, thus demonstrating weak cooling performance under the standard conditions of $Re = 1013$ and $q = 5000$ W m^{-2}. The four MPSFFs (Models B–E) and the conven-

tional spiral flow-field (Model F) exhibit small T_{max}, ΔT, and U_T, which indicates improved cooling performance. The spiral flow-field and the four MPSFFs are found to require a larger pressure drop for a given *Re* number than the conventional serpentine flow-field. The best cooling performance is obtained with a MPSFF of Model E, which shows a 40–60% reduction in the uniformity indices of ΔT and U_T compared with the conventional serpentine flow-field. The effects of flow velocity and heat flux were also analysed. The temperature uniformity indices T_{max}, ΔT and U_T decrease somewhat linearly as the Reynolds number is increased or the heat flux is decreased.

Acknowledgement

The authors gratefully acknowledge the support from Hyundai Motors Co. through Next Generation Vehicle Technology Co. (NGVTEK.com).

References

[1] J. Larminie, A. Dicks, Fuel Cell Systems Explained, John Wiley & Sons, Chichester, 2000.
[2] R.P. O'Hayre, S.W. Cha, W. Colella, F.B. Prinz, Fuel Cell Fundamentals, John Wiley & Sons, New York, 2006.
[3] J.M. Ogden, M.M. Steinnbugler, T.G. Kreutz, J. Power Sources 79 (1999) 143–168.
[4] N. Djilali, D. Lu, Int. J. Therm. Sci. 41 (2002) 29–40.
[5] A. Faghri, Z. Guo, Int. J. Heat Mass Transfer 48 (2005) 3891–3920.
[6] G. Inoue, T. Yoshimoto, Y. Matsukuma, M. Minemoto, H. Itoh, S. Tsurumaki, J. Power Sources 162 (2006) 81–93.
[7] F.C. Chen, Z. Gao, R.O. Loutfy, M. Hecht, Fuel Cells 3 (2003) 181–188.
[8] J. Choi, Y.H. Kim, Y. Lee, K.J. Lee, Y.C. Kim, J. Mech. Sci. Technol. 22 (2008) 1417–1425.
[9] C. Xu, T.S. Zhao, Electrochem. Commun. 9 (2007) 497–503.
[10] J.H. Nam, K.J. Lee, S. Sohn, C.J. Kim, J. Power Sources 188 (2009) 14–23.
[11] H.O. Pierson, Handbook of Carbon, Graphite, Diamond and Fullerenes: Properties Processing and Applications, Noyes Publications, NJ, 1993.